



**HAL**  
open science

## Seismic monitoring of the Indian Ocean Tsunami.

X. Yuan, R. Kind, Helle A. Pedersen

► **To cite this version:**

X. Yuan, R. Kind, Helle A. Pedersen. Seismic monitoring of the Indian Ocean Tsunami.. Geophysical Research Letters, 2005, 32, pp.L15308. 10.1029/2005GL023464 . hal-00109944

**HAL Id: hal-00109944**

**<https://hal.science/hal-00109944>**

Submitted on 2 Mar 2021

**HAL** is a multi-disciplinary open access archive for the deposit and dissemination of scientific research documents, whether they are published or not. The documents may come from teaching and research institutions in France or abroad, or from public or private research centers.

L'archive ouverte pluridisciplinaire **HAL**, est destinée au dépôt et à la diffusion de documents scientifiques de niveau recherche, publiés ou non, émanant des établissements d'enseignement et de recherche français ou étrangers, des laboratoires publics ou privés.

## Seismic monitoring of the Indian Ocean tsunami

Xiaohui Yuan, Rainer Kind,<sup>1</sup> and Helle A. Pedersen<sup>2,3</sup>

GeoForschungsZentrum Potsdam, Potsdam, Germany

Received 12 May 2005; revised 24 June 2005; accepted 6 July 2005; published 9 August 2005.

[1] The 26 December 2004 Sumatra-Andaman earthquake of Mw 9.3 triggered a massive tsunami in the Indian Ocean. We here report on observations of the Indian Ocean tsunami at broadband seismic stations located on islands in the area. The tsunami induces long-period (>1000 s) signals on the horizontal components of the sensor. Frequency-time analysis shows that the long-period signals cannot be due to seismic surface waves, but that it arrives at the expected time of the tsunami. The waveforms are well correlated to tide gauge observations at a location where both observations are available. To explain the signals we favour tilt due to coastal loading but we cannot at the present stage exclude gravitational effects. The density of broadband stations is expected to increase rapidly in the effort of building an earthquake monitoring system. They may unexpectedly become useful tsunami detectors as well. **Citation:** Yuan, X., R. Kind, and H. A. Pedersen (2005), Seismic monitoring of the Indian Ocean tsunami, *Geophys. Res. Lett.*, 32, L15308, doi:10.1029/2005GL023464.

### 1. Introduction

[2] Tsunamis, which are typically triggered by submarine earthquakes, landslides and volcanic eruptions, are long period ocean gravity waves that travel far distances in the ocean. They usually have a period of 200–2000 s and a speed of 150–250 m/s in the open ocean [Ward, 1989]. Direct monitoring of tsunamis is possible via tide gauge stations located at shorelines of continents and islands [Merrifield *et al.*, 2005]. More recent detection equipment includes ocean bottom pressure gauges [Hino *et al.*, 2001; González *et al.*, 2005]. Satellite altimetry can be used to observe tsunamis only if the satellites pass over the relevant region at the time of tsunami [Okal *et al.*, 1999; Gower, 2005]. GPS detections of ionospheric disturbances, created by tsunami induced acoustic waves, are perhaps very promising for tsunami monitoring [Artru *et al.*, 2005].

[3] Tsunamis are also expected to induce coupling with the solid Earth, which can be detected seismically. High-frequency signals have in one case been suggested to result from a tsunami [Pino *et al.*, 2004]. Coupling of ocean disturbances with the solid Earth has been reported and analysed for a long time and is one of the main sources of seismic noise [see Friederich *et al.*, 1998, and references

therein]. Ocean generated noise normally has strong energy at periods shorter than 20 s. Tsunamis on the contrary have very long periods (up to at least 2000 s) and wavelengths up to 500 km [Ward, 1989]. Coupling between atmospheric waves and the solid Earth in the same period range has been reported and modelled by Neumann and Zürn [1999]. We analyse seismograms from permanent broadband seismic stations located in the Indian Ocean and surrounding continents for possible indications of the Indian Ocean tsunami created by the Sumatra-Andaman earthquake of Mw 9.3 [Stein and Okal, 2005; Park *et al.*, 2005]. The station locations are shown in Figure 1. The stations are part of different permanent global or regional seismic networks (IRIS [Butler *et al.*, 2000], GEOSCOPE [Romanowicz *et al.*, 1984], GEOFON [Hanka *et al.*, 2000]) and are equipped with Geotech Borehole KS54000, Streckeisen STS1 or STS2 broadband seismometers.

### 2. Observations

[4] Figure 2 shows the radial (i.e., in the direction toward the earthquake epicenter) component of ground acceleration

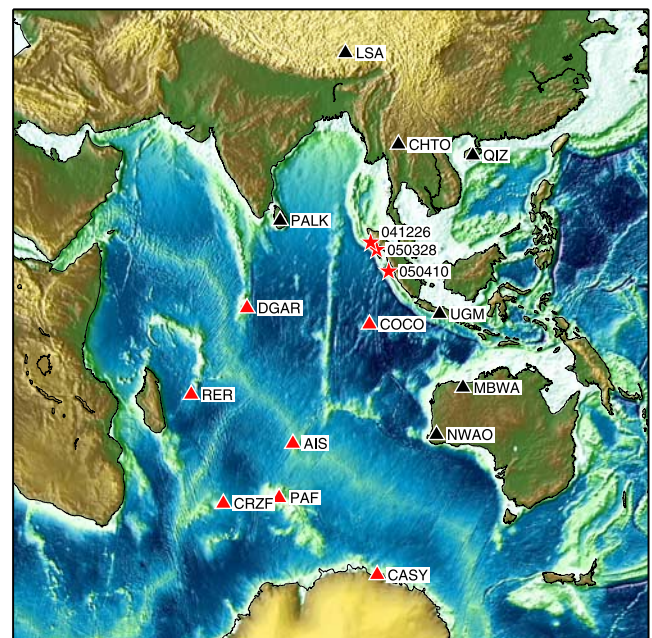


**Figure 1.** Map of the seismic stations in the Indian Ocean and surrounding continents used in this study. The topography of the land and seabed is plotted in colour. Red stars denote epicenters of the three big earthquakes near west coast of Sumatra. Red triangles are ocean stations located on islands or near the coast and which have recorded the tsunami. Black triangles are continent stations without tsunami induced seismic signals.

<sup>1</sup>Also at Department of Earth Sciences, Freie Universität Berlin, Berlin, Germany.

<sup>2</sup>Also at Department of Mathematics and Sciences, Universität Potsdam, Potsdam, Germany.

<sup>3</sup>Also at Observatoire de Grenoble, Laboratoire de Géophysique Interne et Tectonophysique, Université Joseph Fourier, Grenoble, France.

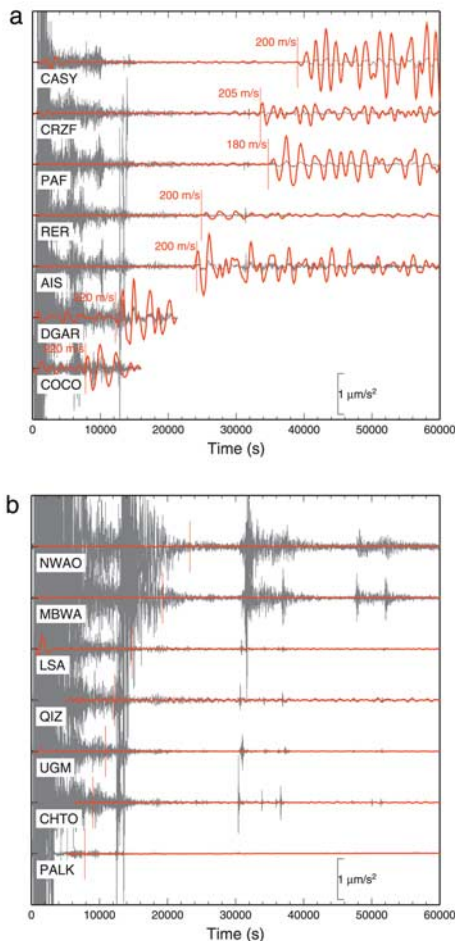


**Figure 2.** Radial-component acceleration seismograms for ocean stations located on islands and near the northern coast of Antarctica (a) and continent stations (b). The accelerations are shown after frequency filtering by two different pass bands (3 pole zero phase Butterworth filter) with lower period bounds of 50 s (thin black lines) and 1000 s (thick red lines). The scale denotes the acceleration on the low-frequency (red) traces while the amplitudes on the high-frequency traces (black) should be multiplied by ten as compared to the scale. The time axis starts at the origin time of the earthquake. The positive amplitude corresponds to motion toward the earthquake. Because station DGAR has a gap in continuous data record at time of  $\sim 22000$  s and station COCO has a disturbing signal at time of 16000 s, we shortened the time window for these two stations. Vertical bars mark the first tsunami arrivals with estimated average speed along the path for each ocean station (a) and a constant speed of 200 m/s for the continent stations (b). Simple models of tsunami propagation using the average ocean depth along the path are able to explain the onset time of the tsunami.

recorded by the stations at long ( $50 < T < 2000$  s) and very long ( $1000 < T < 2000$  s) periods. The 'ocean stations', located on islands and near the coast, have recorded signals related to the long-period tsunami (Figure 2a) while the continent stations have not (Figure 2b). The peak to trough amplitudes (Figure 2) on the radial component of

the tsunami induced seismic signal is between 0.3 and  $3 \mu\text{m/s}^2$ . At periods longer than 2000 s, the tsunami induced seismic signal is still present, but distorted by noise at some stations. The maximum acceleration observed on the radial component at periods shorter than 2000 s is therefore a lower bound on the amplitude of the tsunami induced seismic signal. On average the power spectra of ocean and continent stations are different for periods longer than approximately 500s. The particle motion was elliptical rather than linear in the direction of maximum amplitude. For each station, the amplitude ratio between the direction of maximum and minimum amplitude was of the order 2–5.

[5] The seafloor topography significantly changes the direction of the maximum amplitude, which does not for any ocean station coincide with the direction of motion towards the earthquake epicenter. Detailed maps (Figure 3) of the coastline close to the stations show that the maximum amplitudes generally are perpendicular to the coastline. The maximum amplitude of the acceleration is not simply related to the directivity effect of the tsunami. The 26 December 2004 Indian Ocean tsunami propagated with a maximum strength perpendicular to the Sumatra trench and a minimum parallel to it [Lomnitz and Nilsen-Hofseth, 2005], but this effect is not observed in the tsunami induced seismic signal: ocean stations south-south-east of the earthquake epicenter have comparable long-period amplitudes to those of stations located west of the epicenter, and the displacement varies significantly over relatively short distances (compare for example CRZF and PAF). On the other hand, the distance to the coast is crucial to the amplitude. Only stations less than about 10 km from the shore seem to have strong tsunami induced seismic signals. Station PALK, located 100 km inland in Sri Lanka

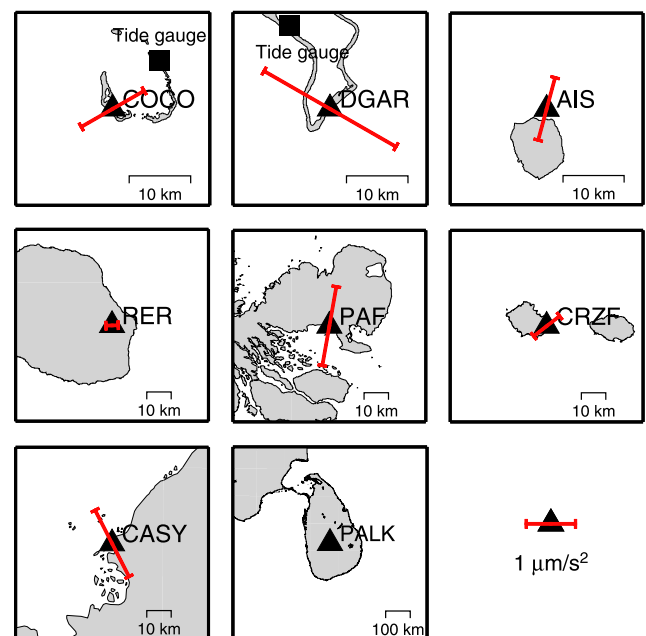


**Figure 3.** Coastline geometry close to the ocean stations (triangles). The red lines show the direction and amplitude of the maximum tsunami induced seismic signal, according to the scale in the lower right corner. The tide gauge position is shown by a solid square.

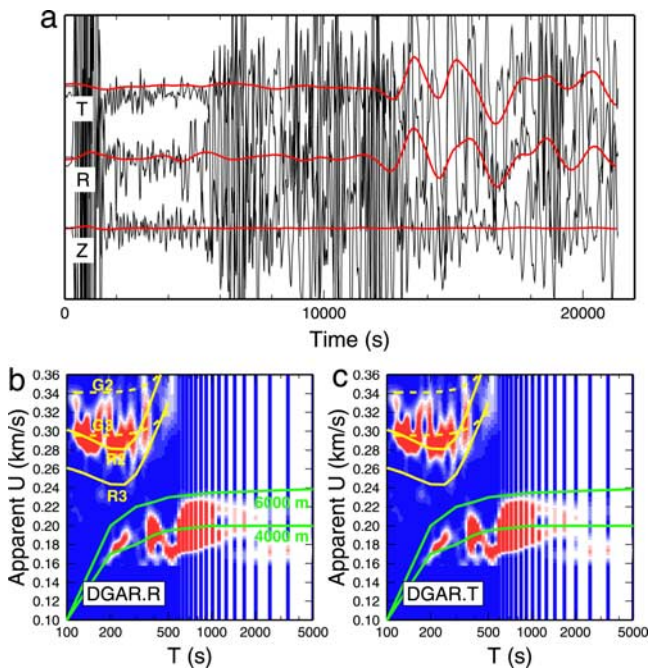


**Figure 4.** (a) Original three-component velocity seismograms of station DGAR rotated into ZRT components and low-pass filtered to 100 s (black lines) and 1500 s (red lines), respectively. The amplitudes are plotted in the same scale. The tsunami is clearly seen at the two horizontal components. (b)–(c) The output of the multiple filter analysis [Dziewonski *et al.*, 1969]. Yellow lines are global average group velocity dispersion curves of fundamental-mode minor-arc and great-arc Rayleigh (solid lines, R2 and R3) and Love waves (dashed lines, G2 and G3), respectively for a standard Earth model (AK135) [Kennett *et al.*, 1995]. The real velocities of the surface wave have been converted into arrival times and further into apparent velocities by using the epicenter-station distance. Green lines are tsunami dispersion curves from Ward [1989] for water depths of 4000 and 6000 m, respectively.

did not record tsunami induced seismic signals, even though the tsunami was very strong on the east coast of the island, causing tremendous damage. The absence of energy on the vertical component and the rapid decay from the coast means that the tsunami induced seismic wave signal may not be related to a propagating seismic wave.

[6] The onset of the tsunami induced signal is indicated as a vertical line in Figure 2a. These observed arrival times of the tsunami agree well with the expected average tsunami speed of approximately 200 m/s for water depth of 4000 to 5000 m [Ward, 1989]. The small differences in the tsunami speed reflects the difference in the average water depth along the path as tsunamis travel faster in deeper than in shallower water. For example, station PAF has a shallower water path than station CRZF, and therefore has a delayed tsunami arrival.

[7] Two mechanisms can possibly explain the observed large tsunami induced seismic signals. Sea level changes will cause changes of gravitational effect to seismometers and/or tilt of island and coastal area. Both effects are likely to exist simultaneously. However, because the apparent

direction of motion for almost all the stations appears to be perpendicular to the shoreline, the latter seems to be the dominant mechanism. The observed maximum accelerations could be caused by a tilt of approximately 0.4 micro radians. The effect of tilt would be very small on the vertical component [Wielandt and Forbriger, 1999; Wielandt, 2002].

[8] In Figure 4 we show three-component seismograms of an ocean station (DGAR). For reference, the original velocity seismograms, rotated into ZRT components and low-pass filtered using a corner frequency of 100 s and 1500 s, are shown in Figure 4a. As in Figure 2, the higher frequency data show mainly fundamental- and higher-mode surface waves, while significant tsunami induced signals are clearly seen on the two horizontal components with a dominant period of over 2000 s. Significant energy is present on the transverse component as well while the vertical component shows no significant long period energy related to the tsunami. These long period waves are not related to seismic surface waves which have travelled paths of varying length, as can be seen through frequency-time analysis. To exclude that the long-period signal is due to seismic surface waves, we applied multiple filter analysis [Dziewonski *et al.*, 1969] to the horizontal records of the broadband seismic stations. Figures 4b and 4c show the result of the multiple filter analysis to data from station DGAR. The signals below 500 s period are dominated by seismic surface waves (reference curves: yellow lines) while the longer periods are dominated by tsunami induced waves (reference curves: green lines).

### 3. Discussion

[9] The tsunami induced seismic signals compare surprisingly well with signals from tide gauges on the two islands where both types of recordings were available

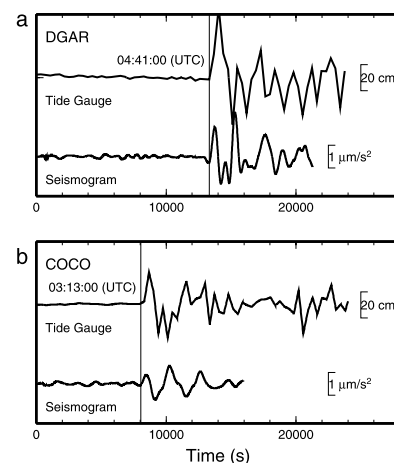


**Figure 5.** Comparison of acceleration seismograms (after low-pass filtering by a 3 point causal Butterworth filter, 1000s corner period) with tide gauge data at stations (a) DGAR and (b) COCO. The seismograms are rotated into the direction of the maximum amplitudes, which are N150°E for DGAR and N60°E for COCO. The time axis starts at the origin time of the earthquake. Scale denotes the displacement for the tide gauge data and acceleration for the seismic data.

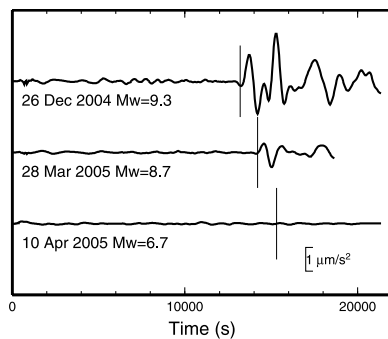


**Figure 6.** Comparison of 1000-s acceleration seismograms (for filtering: see caption to Figure 5) at station DGAR for three earthquakes at approximately the same location (west of Sumatra), but with different magnitudes. The seismograms are rotated into the optimal direction of the tsunami induced motion for station DGAR ( $150^\circ$ ). For each trace, the time axis starts at the earthquake origin time. Note the decrease in amplitude of the tsunami induced signal as the magnitude decreases.

(Figure 5). The onset time and initial waveform are the same, but the tide gauge signal shows increasing complexity with time. The differences may be explained by the complex and non-linear effects that influence the tide gauge [González *et al.*, 1991; Hino *et al.*, 2001] while seismic tsunami observations possibly reflect signals integrated over a larger area, and may also be influenced by the local subsurface structure.

[10] The scaling of the tsunami induced seismic signal is illustrated in Figure 6. Very long-period pulses are present at the expected tsunami arrival of the large earthquake of 28 March 2005 while no very long-period energy is present for the 10 April event which is of much smaller magnitude. Once all the recordings are available for these events, it may be possible to verify how the amplitude of the tsunami induced signals scales with the earthquake magnitude, as they may be influenced by other factors as well, such as focal mechanism and rupture dynamics.

[11] Even though much remains to be understood about tsunami induced seismic signals, the observation of such signals from the Indian Ocean tsunami of 26 December 2004 is unambiguous. It shows that high quality seismic broadband stations can be used not only for determination of earthquake parameters, but also for tsunami detection. The amplitude decay of the tsunami induced seismic signals with distance to the coast therefore imposes important constraint to take into account in the design of the seismic networks for early warning systems.

[12] **Acknowledgments.** We thank Walter Zürn, Günter Asch, Karl-Heinz Jäckel, Rongjiang Wang and Jochen Zschau for discussions on mechanism of tsunami induced seismic signals; Marianne Bruneton for reference dispersion curves, and Stefan Sobolev for discussions about

tsunami simulations. We are grateful to IRIS, GEOSCOPE and GEOFON for providing seismic data and the West Coast/Alaska Tsunami Warning Center and the Sea Level Center, University of Hawaii for providing the tide gauge data. HAP benefited from a fellowship of the Alexander-von-Humboldt Foundation. T. Forbriger and an anonymous reviewer provided thoughtful and constructive reviews.

## References

- Artru, J., V. Ducic, H. Kanamori, P. Lognonné, and M. Murakami (2005), Ionospheric detection of gravity waves induced by tsunamis, *Geophys. J. Int.*, **160**, 840–848.
- Butler, R., et al. (2000), The global seismographic network surpasses its design goals, *Eos Trans. AGU*, **80**, 225–229.
- Dziewonski, A., S. Bloch, and N. Landisman (1969), A technique for the analysis of transient seismic signals, *Bull. Seismol. Soc. Am.*, **59**, 427–444.
- Friederich, A., F. Krüger, and K. Klinge (1998), Ocean-generated microseismic noise located with the Gräfenberg array, *J. Seismol.*, **2**, 47–64.
- González, F. I., C. L. Mader, M. C. Eble, and E. N. Bernard (1991), The 1987–88 Alaskan Bight tsunamis: Deep ocean data and model comparisons, *Nat. Hazards*, **4**, 119–139.
- González, F. I., E. N. Bernard, C. Meinig, M. C. Eble, H. O. Mofjeld, and S. Stalín (2005), The NTHMP tsunameter network, *Nat. Hazards*, **35**, 25–39.
- Gower, J. (2005), Jason 1 detects the 26 December 2004 tsunami, *Eos Trans. AGU*, **86**, 37–38.
- Hanka, W., A. Heinloo, and K.-H. Jaeckel (2000), Networked seismographs: GEOFON real time data distribution, *ORFEUS Electron. Newsl.*, **2**, p. 24. (Available at <http://www.orfeus-eu.org/newsletter/vol2no3/geofon.html>.)
- Hino, R., Y. Tanioka, T. Kanazawa, S. Sakai, M. Nishino, and K. Suyehiro (2001), Micro-tsunami from a local interplate earthquake detected by cabled offshore tsunami observation in northeastern Japan, *Geophys. Res. Lett.*, **28**, 3533–3536.
- Kennett, B. L. N., E. R. Engdahl, and R. Buland (1995), Constraints on seismic velocities in the Earth from traveltimes, *Geophys. J. Int.*, **122**, 108–124.
- Lomnitz, C., and S. Nilsen-Hofseth (2005), The Indian Ocean disaster: Tsunami physics and early warning dilemmas, *Eos Trans. AGU*, **86**, 65–70.
- Merrifield, M. A., et al. (2005), Tide gauge observations of the Indian Ocean tsunami, December 26, 2004, *Geophys. Res. Lett.*, **32**, L09603, doi:10.1029/2005GL022610.
- Neumann, U., and W. Zürn (1999), Gravity signals from atmospheric waves and their modeling, *Bull. Inf. Marees Terr.*, **131**, 10,139–10,152.
- Okal, E. A., A. Piatanesi, and P. Heinrich (1999), Tsunami detection by satellite altimetry, *J. Geophys. Res.*, **104**, 599–615.
- Park, J., et al. (2005), Global seismographic network records the great Sumatra-Andaman earthquake, *Eos Trans. AGU*, **86**, 57–61.
- Pino, N. A., M. Ripepe, and G. B. Cimini (2004), The Stromboli Volcano landslides of December 2002: A seismological description, *Geophys. Res. Lett.*, **31**, L02605, doi:10.1029/2003GL018385.
- Romanowicz, B., M. Cara, J. F. Fels, and D. Rouland (1984), Geoscope: A French initiative in long period three component seismic networks, *Eos Trans. AGU*, **65**, 753–754.
- Stein, S., and E. A. Okal (2005), Speed and size of the Sumatra earthquake, *Nature*, **434**, 581–582.
- Ward, S. N. (1989), Tsunami, in *The Encyclopedia of Solid Earth Geophysics*, edited by D. E. James, pp. 1279–1292, Van Nostrand Reinhold, Hoboken, N. J.
- Wielandt, E. (2002), Seismometry, in *International Handbook of Earthquake and Engineering Seismology*, edited by W. H. K. Lee et al., pp. 283–304, Elsevier, New York.
- Wielandt, E., and T. Forbriger (1999), Near-field displacement and tilt associated with the explosive activity of Stromboli, *Ann. Geofis.*, **42**, 407–416.

R. Kind, H. A. Pedersen, and X. Yuan, GeoForschungsZentrum Potsdam, Telegrafenberg, D-14473 Potsdam, Germany. (yuan@gfz-potsdam.de)